Pharmaceutical Research, Vol. 23, No. 10, October 2006 (© 2006)
DOI: 10.1007/s11095-006-9072-8

Research Paper

Percolative Transport and Cluster Diffusion Near and Below the Percolation Threshold of a Porous Polymeric Matrix

Jayne E. Hastedt[1,3] and James L. Wright[2]

Received January 14, 2006; accepted May 22, 2006; published online August 24, 2006

Purpose. The purpose of this research was to develop a quantitative mass transport model to describe the release of a drug from a porous inert matrix dosage form near and below the percolation threshold for the system.
Methods. Cumulative release profiles were generated for a series of tablets composed of a binary mixture of varying amounts of non-conducting (poly(vinyl stearate)) and conducting (benzoic acid) components. The porous microstructure was analyzed using re-constructed three-dimensional images of leached microtomed tablet sections. Poly(vinyl stearate) was characterized for transport properties, molecular weight and thermal properties.
Results. Based on percolation theory, the binary matrix was determined to have a percolation threshold of 0.09 ± 0.02. Transport, which could not be explained by "classical" percolation theory or surface diffusion alone, was observed below the percolation threshold for the system.
Conclusions. A model describing transport near and below the percolation threshold in matrices composed of two phases, polymer and drug, was developed. The percolation model developed accounts for diffusion within the porous structure and through the inert, insoluble polymeric amorphous regions of the matrix. The low percolation threshold and subsequently high coordination was concluded to be due to the biphasic classical porous and nonclassical polymeric diffusional transport mechanisms associated with the system studied.

KEY WORDS: biphasic conductivity; diffusion; matrix release; percolation theory; porous microstructure.

INTRODUCTION

Transport of material through porous media using principles based on percolation theory has attracted the attention of the pharmaceutical field at a growing rate over the past 10 to 15 years (1–4). For the pharmaceutical formulation scientist, the transport characteristics of a drug entity diffusing through a porous delivery system contribute to both the drug release rate and cumulative amount of drug delivered (5–9). The ability to control and understand the transport from a dosage form is therefore a crucial step in understanding product viability and is required to define the knowledge space linking product development to commercial product performance for controlled release dosage forms.

In an inert, hydrophobic porous matrix, the physicochemical properties of the drug entity alone do not dictate transport. In addition to the contributions from the physicochemical properties of the matrix excipients themselves, the underlying morphology of the matrix plays an important role in defining the transport kinetics. Characterization of the morphology, a combination of topology and geometry of the pore space, is crucial to understanding transport through such systems. Mathematically derived network models, percolation theory being one, are being used more frequently in the pharmaceutical industry to provide insight into the connection between morphology and transport (1,10–14), product development and scale-up (15), compression and compaction (16–19) and implants (20,21).

Percolation theory, being a mathematically derived model, was developed using computer-simulated infinite-sized networks. Much work has been done to correlate the universal parameters derived from the infinite-sized systems of percolation theory to transport through finite-sized systems. The impact of finite size scaling has been demonstrated mainly using computer simulations, although some experimental systems have been studied (22). When a finite-sized system approaches the percolation threshold deviations are expected from theory due to scale differences and can be manifested in variable transport parameters for the matrix (23–27).

The objective of this research was to develop a quantitative transport model that described the release of a drug entity from a porous inert hydrophobic polymeric delivery system over the experimental ranges investigated. This current study is an extension of earlier work that analyzed transport above the percolation threshold for the same system (1,28) and

[1] Global Chem Pharm, ALZA Corporation, 1010 Joaquin Road, Mountain View, California 94043, USA.
[2] Pharmaceutical Development, Infinity Pharmaceuticals, Cambridge, Massachusetts, USA.
[3] To whom correspondence should be addressed. (e-mail: jhastedt@alzus.jnj.com)

focuses on the correlation between morphology and transport near and below the percolation threshold. In this study, an understanding of the transport in heterogeneous materials (through both polymer and pore structure) and the effect of pore morphology on transport were evaluated using percolation theory. The model developed specifically addresses situations where the molecule may diffuse through both water-filled pores (the conducting phase) and through the polymer matrix (classically considered the non-conducting phase) (29).

MATERIALS AND METHODS

Materials

Benzoic acid, 99+% gold label purity ACS reagent grade, was obtained from Aldrich Chemical Company Inc. of Milwaukee, WI. Poly(vinyl stearate); 4-fluorobenzoic acid, 99% purity; acetic acid, 99.8+% ACS reagent gold label purity; and HPLC grade benzene were also purchased from Aldrich. Aerosol OT (sodium dioctyl sulfosuccinate, 10% solution) was obtained from Anderson Laboratories of Fort Worth, TX. Solvents for the HPLC system were purchased from American Burdick & Jackson Co. of Muskegon, MI and consisted of high purity HPLC grade methanol. "Baker Analyzed" reagent grade concentrated HCl from J.T. Baker Chemical Co. of Philipsburg, NJ was used to adjust the buffer solution pH. Potassium chloride, analytical reagent (AR), was purchased from Mallinckrodt of Paris, KY. Benzoic acid and poly(vinyl stearate) were micronized by Sturtevant Mill Company to a particle size of 10.3 and 12 μm, respectively. Properties of the materials as determined from previous research are shown in Table I (1).

Methods

Drug Release

The cumulative release of benzoic acid (BA) from a tablet matrix composed of a binary mixture of micronized poly(vinyl stearate) and benzoic acid was measured using a rotating disk method (100 rpm) and a Distek 2000 dissolution apparatus equipped with an autosampler (Distek Inc., Somerset, NJ) at 37°C in pH 2.0 HCl acid buffer containing the internal standard 4-fluorobenzoic acid (FBA) and 0.25 mM Aerosol OT. The medium was degassed by heating to 50°C and was replaced after every other sample pull point (sample volume = 4.7 ml).

A Carver Laboratory press, Model C, was used to compress the micronized materials into tablets within dies (12.8 mm diameter). Compressional force applied was approximately 5 kN with as short a dwell time as feasible in a manual mode and resulted in tablets of thicknesses ranging from 34 to 40 mm for these studies. Six Hastelloy Alloy G-3 (Corrosion Materials Inc. of Baker, LA) dies of rotating disk design and six 316 stainless steel/Hastelloy shafts were manufactured by the Physics Department machine shop of the University of Wisconsin-Madison. The rotating disk dies were manufactured with five 0.5 mm deep by 0.5 mm wide grooves spaced 1.5 mm apart within the die to prevent the flow of dissolution medium along the edges of the tablets during the experiments. The volume attributed to the total number of grooves covered by the tablets was also incorporated into this volume calculation based on a value of 0.0104 cm^3/groove. Porosities were calculated based on the total benzoic acid content and residual porosities determined by the difference between geometrically calculated volumes and mass-based volumes. Residual or intrinsic porosities ranged from 0.00 to 0.02. A summary of these parameters are provided in Table III along with the transport results from these studies.

Table I. Properties of Poly(vinyl stearate) and Benzoic Acid (1,28)

Component	Diameter (μm)	Density (g/cm^3)	Solubility (mg/ml)	Diffusion Coefficient (cm^2/s)
Poly (vinyl stearate)	10.3	0.98	n/a	n/a
Benzoic acid	12	1.27	4.6	$1.29 \pm 0.05 \times 10^{-5}$

Dissolution samples were analyzed for benzoic acid content by high pressure liquid chromatography (HPLC) using 4-fluorobenzoic acid as an internal standard. The HPLC system consisted of a Beckman Model 160 UV detector equipped with a 254-nm filter, a Model 110 pump, a Rheodyne 7120 injection valve (20-μl injection loop), and Altex Ultrasphere ODS (5 μm, 4.6-mm × 25-cm) column and matched precolumn, and a Kipp and Zonen BD 40 chart recorder. The mobile phase was composed of 65% methanol, 34% purified water, and 1% glacial acetic acid.

Imaging of the Porous Microstructure

Three tablets were sectioned using a microtome (Ultra-Cut E, Reichert-Jung) and photomicrographs were taken (Olympus Model BH-2, 50× objective and 35 mm Olympus camera). All three tablets were extracted during drug release experiments prior to sectioning and represented drug loads of $\emptyset^A = 0.051$, 0.141, and 0.263, where $\emptyset^A$ is the volume fraction accessible which is the sum of volume fraction due to drug load of benzoic acid in the tablet matrix and the inherent porosity of the matrix. Each tablet was mounted on an individual stainless steel chuck using cyanoacrylate adhesive. The tablet and chuck assembly were placed in the microtome and 30 μm of material was removed from each tablet prior to imaging to ensure a flat surface. Due to the brittleness of the microtomed slices, the process was a destructive one and photomicrographs were taken of the portion of the tablet remaining after sectioning slices 8.33 μm in thickness.

The microscope was equipped with a telescope eyepiece, square grid reticle, an X–Y micropositioner stage, and the 35 mm camera. Through-the-lens illumination was employed. Reconstructions were compiled from the images. The square grid was imaged onto the film plane over the tablet surface and a stage micrometer with 10 μm divisions was utilized to calibrate the grid spacing. At 50× magnification the grid spacing was determined to be 16.7 μm. Therefore, microtoming was undertaken at thicknesses equivalent to two slices per square.

After a section was microtomed from the tablet surface, the stainless steel chuck/tablet assembly was removed from the microtome and placed into a mounting slot on the X–Y

micropositioner stage. Three positions, approximately in the midsection of each tablet, were recorded in terms of *x*- and *y*-coordinates from the micropositioner and photographs were taken at each of these positions. The stainless steel chuck/tablet assembly was then removed from the positioning stage and placed back in the microtome. After realignment, another 8.33 μm was removed from the surface and the photomicrograph procedure was again repeated, taking a photograph of the same positions on the tablet surface, but 8.33 μm deeper. A total of 21 slices (174.93 μm) were removed from two of the tablet surfaces and ten slices (83.33 μm) were removed from the highest drug load tablet surface.

Images were recorded on Kodak Technical Pan 2415 135-36 Professional film at ASA 160 and an exposure adjustment of 2.00. An LBD filter was placed in the lighting tube in the position closest to the microscope objectives. The through-the-lens illumination power was set at 6 V and the aperture on the light tube was approximately 25% open to enhance contrast. The exposed film was developed using Kodak D-19 (1:2) developer in order to attain the highest contrast possible. This exposure setting and the processing conditions, as recommended by Kodak (30) produce a high contrast index of 2.70.

Negatives were printed on 8 × 10 Kodak Polycontrast III Type RC FM paper using approximately F5 filtering for high contrast. Burning and dodging techniques were employed in order to eliminate shadows and flashing.

The photomicrographs of the sections were digitized using software and a digitizing tablet (PC3D, Jandel Scientific and Numonics digitizing tablet). Three-dimensional reconstructions of 100 × 100 × 167 or 83 μm were generated. Porosities of the images were calculated using the PC3D software and compared to the experimental values (Table IV).

Characterization of Poly(vinyl stearate)

Diffusion through Poly(vinyl stearate) Films. The transport properties of the polymer were investigated by preparing cast films of poly(vinyl stearate) and measuring transport of benzoic acid through the films. The experiments were conducted in a diaphragm cell configuration. Analysis was performed by applying Crank's relationship for steady-state transport through a thin film of uniform initial distribution with surface concentrations different (31).

The diffusion cell assemblies were arranged in a diaphragm cell configuration with the receiver solution containing FBA, Aerosol OT, and pH 2.0 buffer, (as in the drug release experiments) and the donor solution composed of the identical receiver solution spiked with benzoic acid. All solutions were maintained at 37°C and the assemblies were rotated at 100 rpm throughout the transport experiments. The donor solution contained 2.15 mg benzoic acid/ml, 1.07 μg FBA/ml and 0.25 mM Aerosol OT in pH 2.0 buffer. The receiver solution contained 1.07 μg FBA/ml and 0.25 mM Aerosol OT in pH 2.0 buffer. Samples were withdrawn starting at day 56 to assure steady-state and then taken every 3 to 4 days for a total of 93 days.

Films were prepared by melting micronized poly(vinyl stearate) in a glass Petri dish on a Thermodyne stirring/hot plate. The melts were poured directly into a heated Hastelloy die, resting on a stainless compression plate, and then placed in a Precision vacuum oven and evacuated for approximately 30 min at 65°C and 90 kPa of vacuum to remove residual entrapped air. The molten films were then removed from the oven and allowed to solidify at room temperature. Thicknesses of films were measured using a micrometer. All polymer film samples were evaluated for integrity by "leak testing" using the diffusion cell assembly. Leak testing was conducted by placing the sample films in the diffusion cell assembly filled with receptor solution at 37°C for 24 h and visibly checked to determine if receptor solution leaked through the films. Diffusion experiments were performed on three non-leaking films.

Molecular Weight Determination. The viscosity average molecular weight was determined based on the Mark–Houwink relationship using coefficients for poly(vinyl stearate) in benzene at 25°C (32) and the experimentally determined intrinsic viscosity of the system. The intrinsic viscosity of poly(vinyl stearate) was determined by extrapolation of reduced viscosities as measured with an Ostwald capillary viscometer of four dilute solutions of polymer in benzene at 25°C. The Mark-Houwink relationship, Eq. (1), for this system is

$$[\eta] = 1.0 \times 10^{-3} \overline{M}_v^{0.65} \tag{1}$$

where [η] is the intrinsic viscosity in units of dl/g, $\overline{M}_v$ is the viscosity average molecular weight of the polymer. The Mark-Houwink coefficients k and a were taken as 0.0010 and 0.65 respectively. The values of the Mark-Houwink coefficients depend upon the nature of the polymer, the nature of the solvent, and the temperature. Based on the results of Burlant and Adicoff, the relationship between intrinsic viscosity and molecular weight was observed to be linear between 1,250 and 5,300 Da using these coefficients for poly(vinyl stearate) in benzene (32).

Thermal Analysis. A Perkin-Elmer Differential Scanning Calorimeter 2 (DSC 2), set at a scan rate of 20°C/min over a temperature range of −43 to 147°C, was used to determine the melting point and the enthalpy of fusion of poly(vinyl stearate).

The sample compartment reservoir was filled with liquid nitrogen approximately 1 h prior to use. Calibration of the instrument baseline was performed over the range utilized in scanning. Samples were weighed using a Mettler H51 balance and accurately transferred to aluminum pans, sealed, and reweighed. A reference cell was also prepared at the same time. The cells, sample and reference, were placed in their respective sample compartments and scanning was initiated.

Drug Release Model Development

Percolation Theory and Porous Diffusion. As discussed in previous studies using this system, a percolation model was successfully developed which described transport above the percolation threshold (1). The starting point for the percolation model development was the Higuchi square root time equation (33,34) which is a pseudo-steady state model used to describe transport through macroporous inert matrices at drug loads above the drug solubility [Eq. (2)]. A schematic representing the transport situation is shown in Fig. 1A.

$$Q = \sqrt{D_B[2A - \varnothing C_s] \cdot C_s t} \tag{2}$$

where Q is the amount of drug released per unit area of the tablet exposed to the solvent, D_B is the bulk diffusion

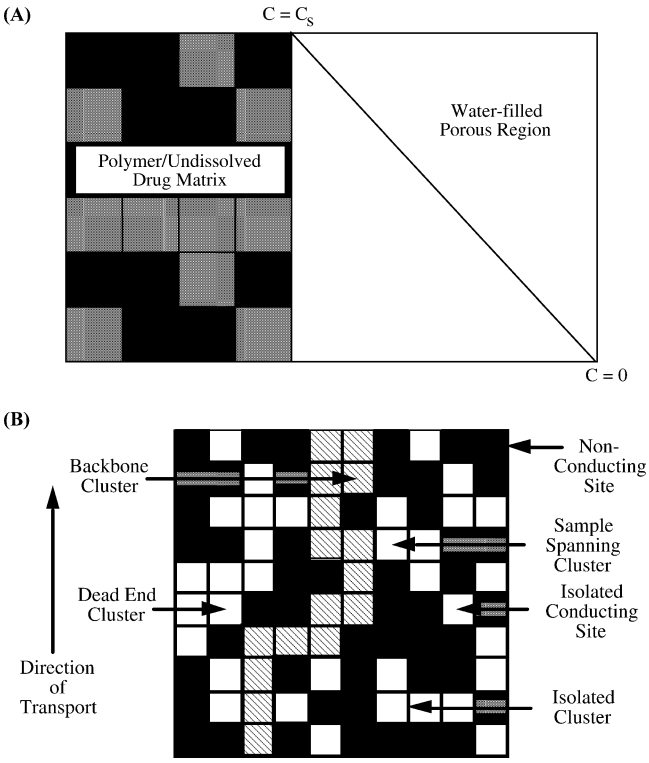

Fig. 1. Diffusional transport model schematics for inert porous matrices. (A) Classical pseudosteady-state model. (B) Classical percolation model and associated parameters.

coefficient describing the diffusion of the drug through the porous structure, A is the concentration of solid drug in the matrix, $\emptyset$ is the porosity of the matrix, C_s is the solubility of the drug in the dissolution media, and t is time.

From Eq. (2) it is apparent that the amount of material released from an inert matrix is proportional to the square root of time with the proportionality constant dependent upon the drug load, solubility, diffusion coefficient, and pore structure. It is assumed that transport does not occur through the polymeric material to any significant degree, that the polymer does not swell during the release of drug, and sink conditions exist outside the matrix.

Higuchi defined the bulk diffusion coefficient by using a tortuosity term (τ), the matrix porosity, and the diffusion coefficient in aqueous media, D_{aq}.

$$D_B = \frac{D_{aq}\emptyset}{\tau} \tag{3}$$

Since the tortuosity factor (that value that indicates how twisting and turning a transport route would be) is not easily related to the material microstructure, investigators have moved to percolation models and other methods to understand the effect that pore structure has on transport (25,26,35,36).

Percolation theory is a mathematical tool that provides a statistical description of the morphology and the associated transport properties of heterogeneous or porous materials by the use of simple scaling laws. The percolative transport characteristics of a porous system provide information about its internal morphology. One of the important advantages percolation theory offers is that it does not use adjustable parameters, such as tortuosity, to describe transport or morphology.

The bulk diffusion coefficient described by Eq. (3), D_B, can be related to the diffusion coefficient of the drug substance in the aqueous media, D_{aq}, by the following relationship

$$D_B = \emptyset^E D_{aq} \tag{4}$$

where $\emptyset^E$ is the relative diffusivity or volume fraction effective. As defined by percolation theory for infinite-sized systems, the value of the relative diffusivity spans the range between 0 and 1 inclusively. The relative diffusivity becomes 1 when $D_B = D_{aq}$, which occurs when the matrix is composed entirely of drug. The relative diffusivity becomes zero when the bulk diffusion equals zero. This situation occurs when no sample-spanning porous pathway exists for the dissolved drug to diffuse along. At low porosities and drug loads, the matrix can contain drug, but the drug is essentially isolated within the matrix, surrounded on all sides by polymer or nonconducting material. In a simple system, the drug cannot transport through the polymer, and therefore transport out of the matrix is not possible without a continuous sample-spanning pore structure. Figure 1B illustrates schematically the relationship between the isolated volume fraction of material, $\emptyset^I$, and another term, the accessible volume fraction, $\emptyset^A$, of an insoluble inert matrix. The accessible volume fraction is simply that volume fraction of the total drug load that is available for transport and comprises what is known as the sample-spanning cluster.

In percolation theory, the critical drug load at which a sample-spanning cluster first traverses the matrix in the direction of transport is known as the critical percolation threshold, $\emptyset_c$. It is in the region near the percolation threshold that percolative scaling laws apply. A nonerodible dosage form formulated above the percolation threshold will permit transport of drug from the matrix. The effect of drug load on these parameters is shown graphically for a theoretical cubic tessellation in Fig. 2 (37,38).

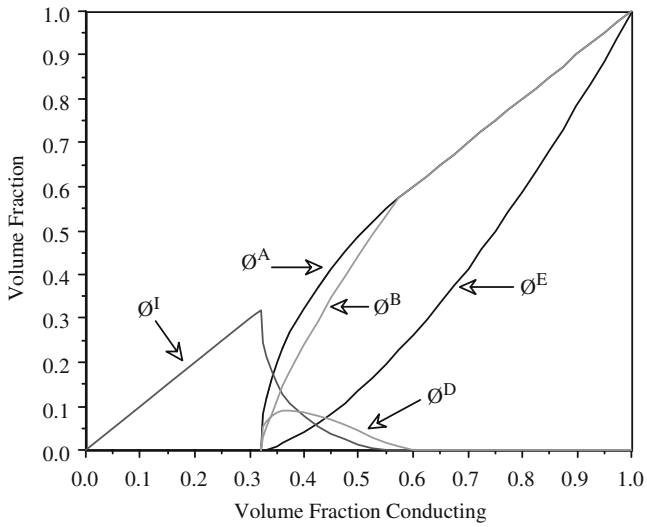

Fig. 2. The effect of drug load on percolation parameters for a cubic tessellation (39,40).

Modifying Higuchi's relationship for percolation parameters and thus eliminating tortuosity, we obtain (1)

$$Q = \sqrt{D_B C_s \left[2\emptyset_d^A \rho - \left(\emptyset_d^A + \varepsilon\right)\right]} t \tag{5}$$

where D_B is described in Eq. (4), $\emptyset_d^A$ is the drug load, ε is the initial, inherent porosity of the matrix, and the other variables are as described previously. Based on Eq. (5), a plot of Q versus square root time will be linear just as in Higuchi's original equation. Also, from the slope of such a line, the value of the bulk diffusion coefficient can be obtained knowing all the other parameters. With the knowledge of D_B and D_{aq} for the system, $\emptyset^E$ can be obtained (Fig. 3A). By conducting these experiments for various values of $\emptyset$, (where $\emptyset = \emptyset_d^A + \varepsilon$) a curve similar to the theoretical profile shown in Fig. 2 for $\emptyset^E$ can be constructed. By following release until the square root time profile plateaus, the volume fraction accessible, $\emptyset_d^A$, can be determined (Fig. 3A).

Percolation Theory and Cluster Diffusion. The physical situation that describes diffusion in the system discussed here is more complex than the simple percolation model previously discussed. For this system, we will develop a model that describes a situation in which the diffusing substance has the ability to not only diffuse through the porous microstructure but also through the polymeric portion of the matrix. To accomplish this, we must account for "hops" that the drug can take across nonporous polymeric regions as it traverses the porous network (39,40). As the drug load within a matrix increases, the porous transport path will become the dominant transport pathway and transport through polymer will become insignificant. Below the percolation threshold transport will be observed only if there is diffusion of drug through the polymer itself, leading to diffusion in a two phase system (29). Thus, an understanding of transport through the heterogeneous matrix needs to take into account two other morphological components of the matrix, the isolated volume fraction or clusters, $\emptyset^I$, and the dead end clusters, $\emptyset^D$ (Fig. 1B). The accessible volume fraction, $\emptyset^A$, is the sum of the dead end clusters, $\emptyset^D$, plus the backbone volume fraction, $\emptyset^B$ [Eq. (7)], and is also equal to the difference between the porosity of the matrix, $\emptyset$, and the isolated volume fraction $\emptyset^I$ [Eq. (8)]. The backbone volume fraction is defined as the tortuous interconnected region of the sample-spanning cluster through which transport is possible. The dead end clusters are extensions off the backbone that are so far removed from the transport path that they do not contribute to transport. Therefore, the dead end clusters, under steady-state conditions, act similarly to the isolated volume fraction in that neither one contributes to transport.

The key assumption made in developing the current model is that isolated and dead end clusters contribute to diffusion near and below the percolation threshold due to the

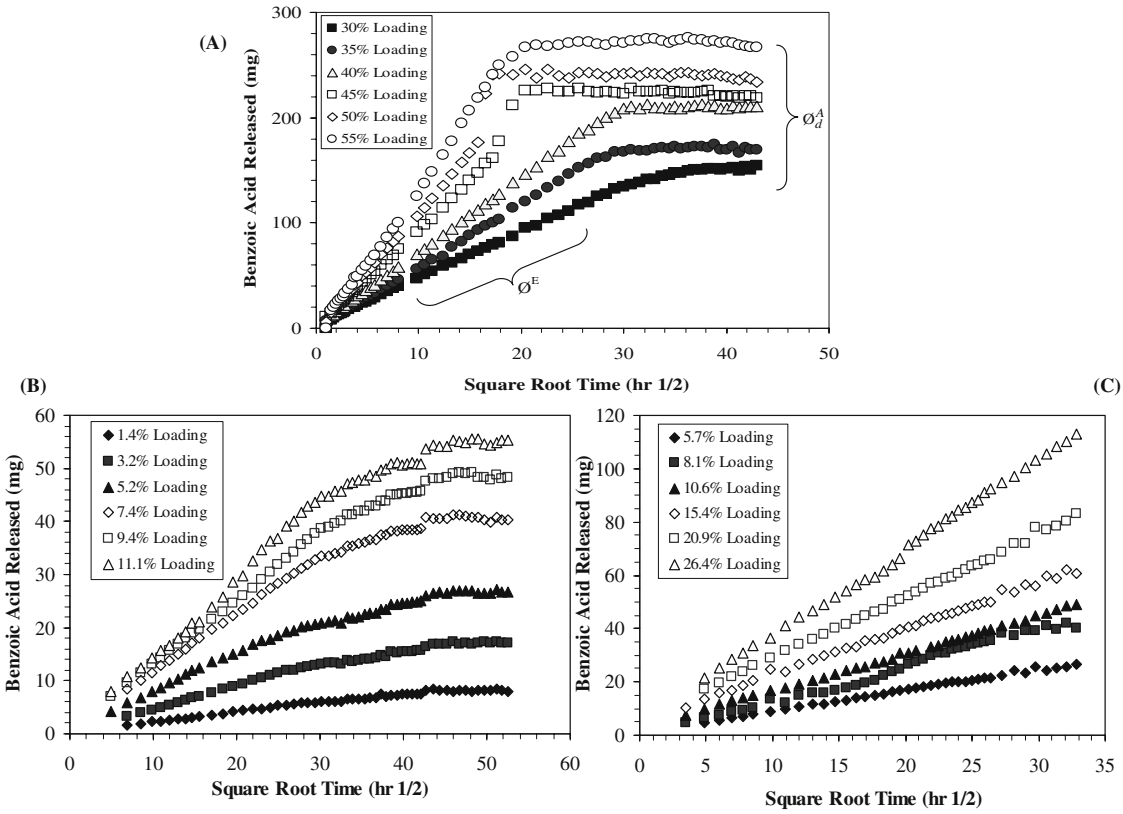

Fig. 3. Cumulative release profiles. (A) Approach for determination of volume fraction effective and accessible drug fraction from experimental cumulative release profiles. (B) Experimental cumulative release profiles as a function of benzoic acid loading near and below the percolation threshold (experiments conducted to complete extraction of benzoic acid). (C) Experimental cumulative release profiles as a function of benzoic acid loading near and below the percolation threshold (experiments not conducted to complete extraction of benzoic acid).

ability of the drug to transport through the inert polymeric matrix. Below the percolation threshold isolated clusters will contribute to transport and above the percolation threshold the porous sample-spanning cluster as well as the dead end and isolated clusters will all contribute to transport through the matrix. A simple first order approximation of the contribution of dead end and isolated pores to transport through porous and polymeric materials is given by Eq. (6).

$$D_B \propto \emptyset^E + \emptyset^D + \emptyset^I \tag{6}$$

And upon substituting the following definitions:

$$\emptyset^D = \emptyset^A - \emptyset^B \tag{7}$$

$$\emptyset^I = \emptyset - \emptyset^A \tag{8}$$

This becomes:

$$D_B \propto \emptyset^E + \emptyset - \emptyset^B \tag{9}$$

where $\emptyset$ is the porosity of the matrix.

Substituting the applicable percolation scaling laws for site percolation models (relationships which express percolation parameters in terms of the difference or "gap" between the porosity and the critical percolation threshold) applicable above the percolation threshold and valid as the porosity approaches the percolation threshold (25).

$$\emptyset^E \propto (\emptyset - \emptyset_c)^{\mu} \tag{10}$$

$$\emptyset^B \propto (\emptyset - \emptyset_c)^{\gamma_b} \tag{11}$$

where μ and γ_b are the universal exponents and therefore known constants for the effective diffusivity and backbone volume fraction [$\mu = 2.0$ (25) and $\gamma_b = 0.9$ (41) for transport in three dimensions]. Substituting these values for the universal exponents and eliminating the proportionality, the following final relationship is obtained

$$D_B = c \cdot (\emptyset - \emptyset_c)^{2.0} + a \cdot \emptyset - b \cdot (\emptyset - \emptyset_c)^{0.9} \tag{12}$$

which is applicable for $\emptyset > \emptyset_c$ and where c, a, and b are proportionality constants.

Equation 12 states that for a system where transport can occur through the polymer as well as through pores, the bulk diffusion coefficient is composed of a continuous pore structure transport component and a heterogeneous transport component (comprised of polymer, dead end and isolated pore clusters). The porous component is the value $c(\emptyset - \emptyset_c)^{2.0}$ derived directly from the volume fraction effective percolation scaling laws as described previously and the heterogeneous transport component, $\left[a \cdot \emptyset - b \cdot (\emptyset - \emptyset_c)^{0.9}\right]$, based on diffusion through isolated pore clusters, polymer and dead end clusters.

Below the percolation threshold, Eq. (12) becomes:

$$D_B = a \cdot \emptyset \tag{13}$$

for $\emptyset \leq \emptyset_c$ which states that the bulk diffusivity below the percolation threshold is a linear function of the drug load. This simplification occurs because of the lack of the classical sample-spanning cluster below the percolation threshold.

Determination of the coordination number of a site (z) in a three dimensional lattice can be calculated based on the empirical relationship shown in Eq. (14) (1,42,43). The coordination is a measure of the complexity of the microstructure and represents the number of nearest neighbors a site has.

$$\emptyset_c = \frac{1}{1 + 0.356z} \tag{14}$$

Based on the model developed above, once the critical percolation threshold is determined, a can be obtained independently from the data set below the critical percolation threshold using Eq. (13). Once a is determined, the two remaining param-

Table II. Volume Fraction Accessible Results

Porosity ($\emptyset$)	Volume Fraction Drug ($\emptyset_d$)	Inherent Porosity (ε)	Calculated Volume Fraction Accessible of Drug ($\emptyset_d^A$)	Calculated Volume Fraction Isolated ($\emptyset^I$)	Volume Fraction Accessible ($\emptyset^A$)
0.021	0.011	0.00	0.012	−0.001	0.021
0.035	0.025	0.01	0.026	−0.001	0.035
0.051	0.041	0.01	0.041	0.000	0.051
0.059	0.059	0.00	0.065	−0.006	0.059
0.094	0.074	0.02	0.077	−0.003	0.094
0.088	0.088	0.00	0.086	0.002	0.088
0.263[a]	0.243	0.02	0.239	0.004	0.263
0.307[a]	0.287	0.02	0.278	0.009	0.307
0.348[a]	0.328	0.02	0.339	−0.011	0.348
0.393[a]	0.373	0.02	0.376	−0.003	0.393
0.440[a]	0.420	0.02	0.420	0.000	0.440
0.490[a]	0.470	0.02	0.471	−0.001	0.490

[a] Data reproduced from previous studies (1,28).
Definitions and calculations: $\emptyset_d^A = \frac{Amnt\ Released\ at\ Plateau}{\rho_{BA} - Volume_{tablet}}$,

$$\emptyset = \emptyset_d + \varepsilon = \emptyset^A + \emptyset^I = \emptyset_d^A + \varepsilon + \emptyset^I$$
$$for\ \emptyset^I = 0,\quad \emptyset = \emptyset_d + \varepsilon = \emptyset_d^A + \varepsilon = \emptyset^A \quad or \quad \emptyset_d = \emptyset_d^A.$$

eters, c and b, can be determined by fitting the applicable data sets above the critical percolation threshold to Eq. (12).

RESULTS

Drug Release

A series of transport experiments were conducted in the realm near and below the percolation threshold for the biphasic system containing benzoic acid and poly(vinyl stearate). The experimental release results are shown in Fig. 3B and C.

Volume fraction accessible results were generated from the plateau of the square root time drug release profiles from six studies (Fig. 3B) as described previously and are tabulated in Table II along with results from earlier studies (1). The volume fraction accessible data are graphically presented in Fig. 4A and compared to theoretical Monte Carlo simulation profiles for different coordination values (z = 6, 8, and 12) from the literature (42).

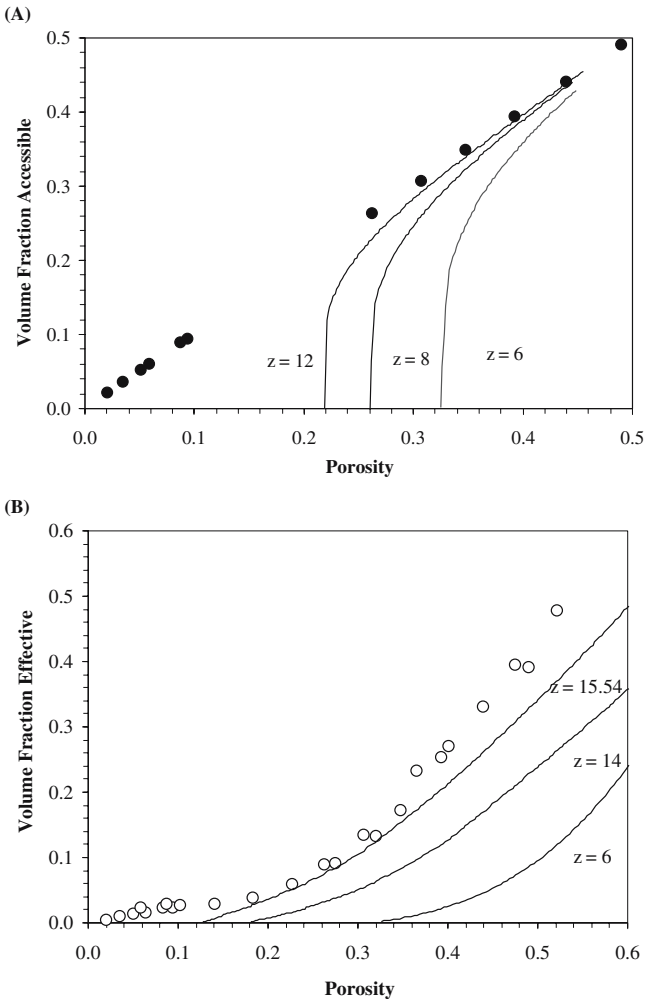

Fig. 4. Experimental volume fraction accessible and effective results compared to theory. (A) Experimental volume fraction accessible results (*closed circles*) compared to literature profiles for the simple cubic lattice (z = 6), body-centered cubic lattice (z = 8) and the face-centered cubic lattice (z = 12) (42). (B) Experimental volume fraction effective results (*open circles*) compared to theoretical simulations for the Voronoi tessellation (z = 15.54), the tetrakaidecaconoic tessellation (z = 14), and the simple cubic lattice (z = 6) (37,44).

Volume fraction effective results were calculated from the initial slope of the cumulative release versus porosity profiles and are tabulated in Table III. The $\emptyset^E$ results are shown graphically in Fig. 4B and are compared to simulated profiles for the Voronoi (z = 15.54) and tetrakaidecahedral (z = 14) tessellations (44) and the simple cubic lattice (z = 6) (37).

Imaging of the Porous Microstructure

Three tablets with volume fractions accessible values of 0.051, 0.141, and 0.263 were imaged to determine their porous microstructures. Twenty-one 8.33 μm thick slices of $\emptyset^A$ = 0.051 and 0.141 were imaged and reconstructions were performed from one location of the tablet surface. Ten 8.33 μm thick slices of $\emptyset^A$ = 0.263 were taken and reconstructed into a three-dimensional images of a portion of the tablet surface.

Figure 5 shows a comparison of the three tablets at dimensions of 100 × 100 × 167 μm for $\emptyset^A$ = 0.051 and 0.141; $\emptyset^A$ = 0.263 has dimensions of 100 × 100 × 83 μm. The back section of each one of the reconstructions is 100 × 50 × 167 or 83 μm while the front section is 100 × 50 × 167 or 83 μm.

From these three-dimensional reconstructions, it can be concluded that the pore structures reproduced by this method depict a complex underlying microstructure. The porous microstructure, with respect to the drug loads analyzed, follows the expected structural trend of arrangement. As the drug load increases, it appears as if larger clusters dominant the matrix microstructure. At the lowest drug loads, on the scale imaged in these studies, isolated clusters appear to dominate, and between the upper and lower drug loads imaged, it appears as if are combination of both small and large clusters exist.

The porosity of each reconstructed section was calculated using Jandel Scientific PC3D software and are shown in Table IV. The results are in relatively good agreement with the actual experimental porosity values for these matrices, indicating that the reconstructions are fairly good representations of the entire tablet matrix.

Characterization of Poly(vinyl stearate)

Viscosity Average Molecular Weight of Poly(vinyl stearate)

Solutions of poly(vinyl stearate) dissolved in benzene were prepared and their "time-to-drain" values were measured with respect to that of pure benzene as described in "Methods". Table V lists the solution concentrations utilized and the resulting drain times, relative drain times and reduced viscosities.

An intrinsic viscosity value of 0.134 dl/g was determined from a plot of the reduced viscosity as a function of concentration. Using the Mark–Houwink relationship stated previously [Eq. (1)] this translates to a viscosity average molecular weight of 1,870 Da. For the repeat unit of poly(vinyl stearate), $(C_{20}H_{38}O_2)_n$, using a calculated molecular weight per repeat unit of 310.4 Da, an average chain length of 6 repeat units per polymer chain can be calculated. These results indicate that poly(vinyl stearate) is more of an

Table III. Summary of Percolation Parameters Obtained from Experimental Results

Porosity ($\emptyset$)	Tablet Thickness (cm)	Volume Fraction Drug ($\emptyset_d$)	Inherent Porosity (ε)	Volume Fraction Accessible ($\emptyset^A$)	Slope $\times 10^5$ ($g/s^{1/2}$)	$D_B \times 10^6$ (cm^2/s)	Volume Fraction Effective ($\emptyset^E$)
0.021	0.398	0.011	0.01	0.021	0.34	0.053	0.004
0.035	0.391	0.025	0.01	0.035	0.76	0.120	0.009
0.051	**0.386**	**0.041**	**0.01**	**0.051**	**1.19**	**0.179**	**0.014**
0.064	0.388	0.044	0.02	0.064	1.30	0.200	0.015
0.059	0.376	0.059	0.00	0.059	1.81	0.289	0.022
0.083	0.380	0.063	0.02	0.083	1.88	0.292	0.023
0.094	0.378	0.074	0.02	0.094	2.07	0.301	0.023
0.088	0.384	0.088	0.00	0.088	2.49	0.367	0.028
0.103	0.376	0.083	0.02	0.103	2.34	0.343	0.027
0.141	**0.370**	**0.121**	**0.02**	**0.141**	**2.88**	**0.356**	**0.028**
0.184	0.366	0.164	0.02	0.184	3.87	0.474	0.037
0.228	0.356	0.208	0.02	0.228	5.51	0.758	0.059
0.263[a]	**0.388**	**0.243**	**0.02**	**0.263**	**7.32**	**1.140**	**0.089**
0.276[a]	0.350	0.256	0.02	0.276	7.56	1.160	0.090
0.307[a]	0.376	0.287	0.02	0.307	9.77	1.730	0.134
0.321[a]	0.356	0.301	0.02	0.321	9.92	1.700	0.132
0.348[a]	0.380	0.328	0.02	0.348	11.82	2.210	0.171
0.366[a]	0.360	0.346	0.02	0.366	14.15	3.000	0.233
0.393[a]	0.364	0.373	0.02	0.393	15.30	3.260	0.253
0.402[a]	0.344	0.382	0.02	0.402	15.98	3.470	0.269
0.440[a]	0.350	0.420	0.02	0.440	18.56	4.260	0.330
0.475[a]	0.340	0.455	0.02	0.475	21.11	5.090	0.394
0.490[a]	0.352	0.470	0.02	0.490	21.33	5.030	0.390
0.522[a]	0.336	0.502	0.02	0.522	24.42	6.170	0.478

Bolded rows indicate tablets used in analysis of microstructure experiments.
[a] Experimental results generated from previous work analyzing diffusion above the percolation threshold (1).

oligomer than a high molecular weight polymer. These results are consistent with characterization studies conducted by other researchers (32,45).

Melting Point and Heat of Fusion of Poly(vinyl stearate)

The results from the DSC scans taken of pure polymer indicated a first order phase transition at 49.4°C with an onset temperature of 41.9°C. The peak spanned a temperature range of 37.4 to 60.3°C and from the area under the curve; the ΔH_{fus} was calculated to be 23.0 cal/g. Scan rate was 20°/min over a temperature range of −13–127°C. Poly(vinyl stearate) sample weight was 11.33 mg of pure, unpurified powder.

Literature values for purified poly(vinyl stearate) indicate a first order phase transition at 51.7°C from refractive index measurements and a range of 50.5–51.2°C from polarizing light microscopy when evaluated under heating conditions (46). The authors of the cited work indicated the presence of a hysteresis effect in either method of evaluation.

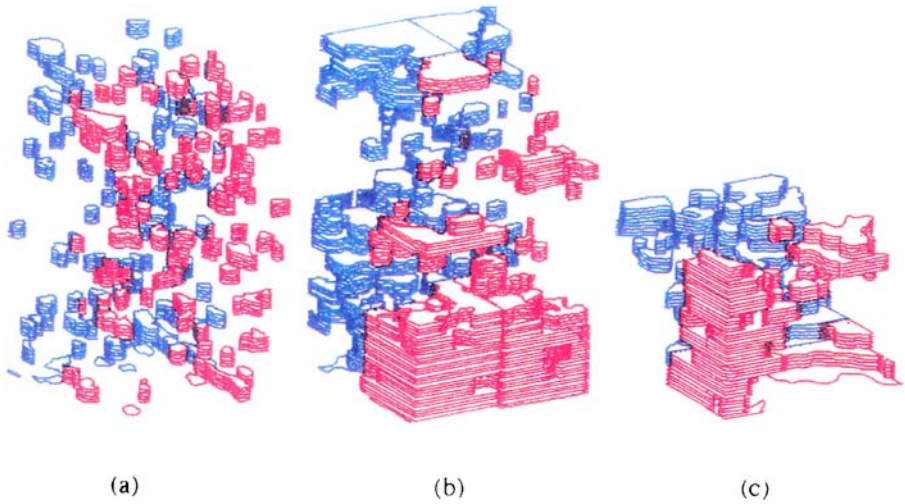

Fig. 5. Experimental three dimensional porous microstructure reconstructions for $\emptyset^A = 0.051$ (a), 0.141 (b), and 0.263 (c). Dimensions are 100 × 100 × 167 μm for $\emptyset^A = 0.051$ and 0.141; $\emptyset^A = 0.263$ has dimensions of 100 × 100 × 83 μm. The back section of each one of the reconstructions is 100 × 50 × 167 or 83 μm and the front section is 100 × 50 × 167 or 83 μm.

Table IV. Comparison of Experimental Porosity Values to Calculated Porosities Based on Porous Microstructure Reconstructions

Volume Fraction Accessible $\emptyset^A$	Software Calculations			Experimental Porosity
	Volume of Polygons (μm^3)	Total Sectioned Volume (μm^3)	Calculated Porosity	
0.051	2.87×10^5	4.88×10^6	0.059	0.051
0.141	8.77×10^5	4.88×10^6	0.180	0.141
0.263	5.66×10^5	2.32×10^6	0.244	0.263

The cooling first order phase transitions were lower melting temperatures; 45.6°C from refractive index work, and a range of 44.0–46.5°C from polarizing light microscopy.

Diffusion through Poly(vinyl stearate) Films

Transport through the polymer was modeled as transport through a thin film of uniform initial concentration with surface concentrations different from Crank (31). In terms of permeability and at steady-state,

$$Q_t = \frac{DC_1}{l} \cdot \left(t - \frac{l^2}{6D}\right) \tag{15}$$

where Q_t represents the total amount of diffusing substance which has passed through the membrane in time t, l is the membrane thickness, C_1 is the concentration of the diffusing species in the donor compartment, and D is the diffusion coefficient.

From Eq. (15), a plot of Q_t versus t has an intercept L_t on the t-axis as given by

$$L_t = \frac{l^2}{6D} \tag{16}$$

from which the diffusion coefficient, D, can be obtained.

Based on experimental results from three independent film samples and the analysis described above, the diffusion coefficient, D, of benzoic acid through films of poly(vinyl stearate) was calculated to be $7 \pm 2 \times 10^{-9}$ cm^2/s at 95% confidence. Table VI summarizes the results from these experiments.

Based on these results, it can be concluded that transport of benzoic acid through the pure polymer is possible.

A summary of the poly(vinyl stearate) material properties determined in the above studies is provided in Table VII.

Table V. Reduced Viscosity Results for Poly(vinyl stearate)/Benzene Solutions at 25°C

Solution Concentration (g/dl)	Drain Time (s)	Relative Drain Time (s)	Reduced Viscosity (dl/g)
0 (pure benzene)	60.1 (0.2)	1.0	n/a
0.409	63.5 (0.1)	1.1	0.139
0.900	67.9 (0.1)	1.1	0.144
1.993	78.7 (0.1)	1.3	0.155
2.961	90.2 (0.1)	1.5	0.169

Extrapolated intrinsic viscosity = $\eta = 0.134$ dl/g
Calc. viscosity avg. mol. wt. ($\boldsymbol{M}_v$) = 1,870 Da

Values in parenthesis are standard deviations based on five evaluations.

DISCUSSION

Diffusion through Poly(vinyl stearate) Films

Based on the transport study results, benzoic acid has the ability to diffuse through pure poly(vinyl stearate) films. Poly(vinyl stearate) is a crystallizable comb-like polymer which is brittle in the solid state. The crystallinity of the solid polymeric material is thought to be due to the hexagonal packing of the side chains of the polymer (47). The transition or melting temperature for the polymer is low and within 10–15°C of the experimental temperature for the studies conducted in this current research. Lutz and Witnauer (48) have shown that poly(vinyl stearate) is approximately 88% crystalline between room temperature and 40°C when measured by XRD. In the realm between 40 and 45°C the amount of crystallinity decreases slightly with temperature to approximately 80%. Above 45°C, the crystallinity drops dramatically as the polymer melts and was immeasurable above 46°C. The processing procedure utilized to reduce the particle size of the poly(vinyl stearate) and the benzoic acid was micronization. The crystallinity of the polymer may have been reduced with this procedure and therefore may have increased the amount of amorphous material in the polymer over the crystalline content that is inherent to the polymer. The water uptake associated with the amorphous regions of a polymer is well documented (49) and in the benzoic acid/poly(vinyl stearate) system these regions would provide a pathway of transport for the water soluble benzoic acid through the polymer itself. If the amorphous nature of the polymer was such that it formed "sample-spanning clusters" spanning the matrix, the benzoic acid could be transported freely either through polymer or pore space in a "skate"/"nonskate" manner (50). The amorphous clusters would not even have to be sample-spanning, if they were large enough to link various section of the porous sample-spanning clusters or even finite pore clusters to produce a "concerted sample-spanning cluster" transport would be enhanced.

Therefore, for the conditions at which the release experiments were conducted and based on the presence of amorphous material inherent to the polymer, transport

Table VI. Benzoic Acid Transport through Poly(vinyl stearate) Cast Films

Film Sample	1	2	3
$D \times 10^8$ (cm^2/s)	0.761	0.897	0.570
Average diffusion through films			$0.74 \pm 0.18 \times 10^{-8}$ cm/s

Confidence intervals calculated from the standard error of the mean at 95% confidence.

Table VII. Summary of Measured Poly(vinyl stearate) Material Properties

Property	Result	Measurement Method
$\bar{M}_v$	1,870 Da	Intrinsic viscosity
T_m	49.4°C	DSC
ΔH_{fus}	23.0 cal/g	DSC
D^a	$0.74 \pm 0.18 \times 10^{-8}$ cm^2/s	Diaphragm cell

[a] Diffusion coefficient.

thorough pure poly(vinyl stearate) is not an unexpected event. It is also anticipated that the presence of Aerosol OT, aided in the transport through the amorphous regions of the hydrophobic polymer by enhancing the wetting of the hydrophobic polymer in the aqueous media.

In terms of classical percolation theory, benzoic acid, as the "conducting" material, has the ability to diffuse through pores. In this research, benzoic acid also has the ability to non-classically transport through the polymer as well. It has been demonstrated that superconducting as well as normal metallic bond systems that exhibit this form of transport behavior in percolation theory can be described in terms of "termite transport" (39,40). A termite has the ability to diffuse slowly (or chew) through the nonconducting phase of the matrix. When the termite encounters a pore, it rapidly traverses the void (or skates) along the porous pathway. The termite then continues on its way again making its way through the classically nonconducting phase, diffusing through the conducting porous pathways, or a combination of the two transport mechanisms.

The Porous Microstructure

The complex microstructure evident at the levels of drug loading imaged is apparent from Fig. 5. The more complex the microstructure of a system, the lower the percolation threshold [Eq. (14)]. The inherently complex nature of the underlying microstructure of the benzoic acid/poly(vinyl stearate) system therefore results in a naturally low percolation threshold which is also influenced by the volume fraction of the non-classically percolating regions of the polymer.

Literature references of percolating systems with low thresholds have been described for systems composed of aluminum oxide fleece and aerogels (51,52). The low threshold values of these systems are generally attributed to oriented microstructures. Even though it is difficult to definitively discern whether or not sufficient orientation or bias exists in the porous three-dimensional reconstructions generated from the systems, very fine chain-like structures appear to exist in the lowest drug load reconstruction. If there were an orientation of the benzoic acid particles, the transport would be characterized as nonuniversal.

Transport Results and the Cluster Diffusion Percolation Theory Model

Determination of the Percolation Threshold

Before analysis of the data using the cluster diffusion percolation model developed here can be conducted, the percolation threshold of the benzoic acid/poly(vinyl stearate) system must be evaluated. The difficulty in determining the threshold from the experimental transport data lies in the lack of classical percolative transport scaling behavior near the threshold. The experimental volume fraction effective profile does not approach zero as the porosity approaches the percolation threshold of the system in the well-defined manner dictated by the universal scaling exponent and the pre-exponential factor.

From the scaling relationships discussed previously, it is evident that a ln–ln plot of the scaling laws will yield a straight line with the slope equal to the universal exponent. If a plot of ln $\emptyset^E$ versus ln $\emptyset$ is constructed, the resulting plot will be linear, indicating that a scaling relationship is evident over the porosity ranges evaluated.

A break in the ln $\emptyset^E$ versus ln $\emptyset$ plot would indicate a transition to another scaling law or transition to another dominating mechanism of transport. Transport mechanisms above and below the percolation threshold of the benzoic acid/poly(vinyl stearate) system should be different as is evident in the developed model. Below the percolation threshold, the dominant form of transport is through poly(vinyl stearate) from isolated pores of drug. Far above the percolation threshold, the dominant form of transport is through the porous channels. In the region close to, but above, the percolation threshold, the transport mechanism consists of a combination of cluster diffusion (isolated and dead end clusters allowing transport from cluster to cluster as well as from cluster to sample-spanning cluster) and percolative transport (transport on the sample-spanning cluster). The ability of the benzoic acid particles to diffuse from an isolated cluster to a sample-spanning cluster or through pure polymer into pockets of pores in a "nonskate"/"skate" manner would be a primary mechanism of transport in this transition region.

The resulting ln–ln plot of the bulk diffusivity data obtained from the transport experiments versus the system porosity is shown in Fig. 6. This plot of the experimental data shows three distinct regions. The first linear region is indicative of scaling below the threshold (isolated cluster diffusion) and

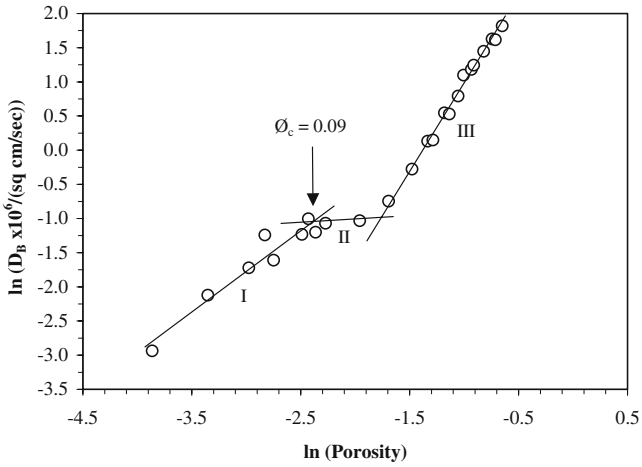

Fig. 6. Determination of the percolation threshold of the benzoic acid poly(vinyl stearate) tablet matrix. The individual points are experimental data. The *solid lines* are regression lines for each region as indicated by the *Roman numerals*. The intersection of the first two regions is taken to be the conducting phase threshold of the system. The percolation threshold was evaluated to be 0.09 ± 0.02 at 95% confidence.

has a slope of 1.2, the third linear region is scaling above the threshold (percolative transport dominating, but cluster diffusion in terms of isolated and dead ends still evident) and has a slope of 2.5. The second region is a transition region between these two where the "skating" on clusters and diffusion through poly(vinyl stearate) occurs. The first break in the ln–ln plot can therefore be taken as the percolation threshold for the classical conducting phase of the system.

Based on linear regression analysis of the regions, the intersection point of regions I and II was determined to be 0.09 ± 0.02 at 95% confidence, which is slightly higher than the percolation threshold originally calculated for this system (1).

The low percolation threshold obtained for this system is therefore a quantity reflecting the complexity of the underlying porous microstructure and the percolating nature of the polymer. Regardless of the transport characteristics of the polymeric phase, the experimentally determined threshold is still lower than the thresholds of the other fairly complex percolating lattice types such as the Voronoi and the tetrakaidecanoic tessellations (Fig. 4B).

Estimation of the Model Parameters

With the determination of the percolation threshold of the system, evaluation of the percolative transport model parameters can be undertaken. Nonlinear multiple regression analysis was carried out on the bulk diffusivity data by using a statistical software package (SYSTAT, Inc., Evanston, IL). Three parameters, one below $\emptyset_c$ and two above $\emptyset_c$, were fit in a two step process using a total of 24 data sets. A table of the statistical results for both above and below the threshold is given in Table VIII.

Model Parameters below the Percolation Threshold. Previously, Eq. (13) was derived to describe transport below the percolation threshold of the system. By fitting Eq. (13) with seven sets of experimental bulk diffusivity versus porosity data, the following result is achieved

$$D_B = 3.8 \times 10^{-6} \cdot \emptyset \tag{17}$$

which is applicable for $\emptyset \leq \emptyset_c$.

Model Parameters near and above the Percolation Threshold. The relationship derived for transport near and above the percolation threshold was given in Eq. (12). Using $\emptyset_c = 0.09$ and $a = 3.8 \times 10^{-6}$, Eq. (12) becomes

$$D_B = c \cdot (\emptyset - 0.09)^{2.0} + 3.8 \times 10^{-6} \cdot \emptyset - b \cdot (\emptyset - 0.09)^{0.9}, \tag{18}$$

where literature values for the universal exponents for conductivity and backbone in three dimensions were used (25,41).

Fitting the remaining 17 sets of data from above $\emptyset_c$, the two variables, c and b, were determined to be $33 \pm 2 \times 10^{-6}$ and $3.9 \pm 0.7 \times 10^{-6}$ respectively. The resulting relationship for percolative transport near and above the percolation threshold is therefore

$$D_B \times 10^6 = 33 \cdot (\emptyset - 0.09)^{2.0} + 3.8 \cdot \emptyset - 3.9 \cdot (\emptyset - 0.09)^{0.9} \tag{19}$$

Comparison to Experimental Bulk Diffusivities

From the release data listed in Table III a plot of the experimentally determined bulk diffusivities versus porosity can be overlaid with the calculated bulk diffusivities determined from the model [Eqs. (17) and (19)]. The agreement between the experimental and calculated results is readily apparent over the experimental range of porosity investigated in this research (Fig. 7).

By using the percolation threshold value of 0.09 and Eq. (14), the coordination for the benzoic acid/poly(vinyl stearate) matrix was determined to be 28 ± 7 based on a 95% confidence interval. The imaged porous microstructure reconstructions indicate a complex microstructure for the system. The overall coordination is most likely a combination of the structural complexity of the porous pathway and the conducting regions of the polymeric phase.

Contributions to Bulk Transport

Percolation scaling theory was developed for infinite-sized systems and the universal scaling constants are derived using computer simulation techniques on infinite-sized networks. In the case of this research, the systems analyzed are not computer simulations, but are real systems that are finite-sized. For finite-sized systems one anticipates deviation from classical percolation theory, especially in the vicinity of the percolation threshold (23–27). Deviations due to either release of benzoic acid from the surface of the tablet and/or finite size scaling would be manifested in the form of variability in the observed bulk diffusion coefficient. As indicated in Fig. 3B and C, transport in the vicinity of the percolation threshold is linear with the square root of time indicating that the diffusion coefficient is not changing with depth. Also, the linearity of the scaling relationship shown in Fig. 6 indicates that contributions from finite size scaling do not appear to be significant. Over the extended release measurement period

Table VIII. Nonclassical Percolative Transport Calculated Model Parameters

Model Region	Fitted Parameter	Model Estimate $\times 10^6$	Std. Error of the Estimate $\times 10^6$	Number of Observations
Near and above the percolation threshold	c	33 (2)	0.9	17
	b	3.9 (0.7)	0.35	17
Below the percolation threshold	a	3.8 (0.6)	0.23	7

Values in parenthesis are 95% confidence intervals.

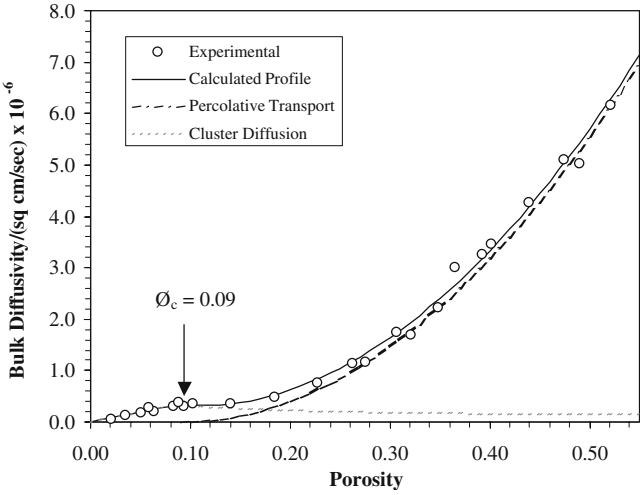

Fig. 7. Comparison of experimental results to percolative transport and cluster diffusion model. *Open circles* are experimental bulk diffusivities, the *solid line* is the calculated profile. *Dashed lines* are the contributions of the percolative transport parameter (volume fraction effective) and the percolative morphological parameters (isolated and dead end clusters).

evaluated, the transport results therefore obey the simple relationship that the diffusion is constant and therefore for the development of this model, we have assumed that there is minimal impact of surface diffusion and/or finite size scaling effects.

Along with the overall calculated profile shown in Fig. 7, the contributions to transport from the morphological clusters of isolated and dead end clusters and the classical percolative transport from the volume fraction effective are calculated using the developed model. The profile is divided into its contributing transport fractions above the threshold, since below the threshold the transport is due to isolated cluster diffusion alone.

From Fig. 7, the morphological contribution to transport assumes a weakly exponential decrease that is indicative of classical cluster size distribution and dead end cluster size behavior above the percolation threshold (25). The percolative transport mechanism is a dominating contributor to transport above the percolation threshold as the cluster diffusion parameter values wane. At regions above the threshold it appears that the dominating mechanism of transport is diffusion along the sample spanning cluster. The slight deviation of the percolative transport mechanism from the total calculated profile is presumably real and is due to the ability of benzoic acid molecules to jump across poly(vinyl stearate) junctions through thin polymer membranes separating pore channels. In this manner, the "skate"/"nonskate" mechanism (39,40) is still operating. The morphological cluster diffusion most strongly influences transport in the region nearest the percolation threshold, as can be concluded from the results presented in this graph.

CONCLUSIONS

The biphasic conducting nature of the tablet matrix resulted in "nonclassical" percolative transport. The ability of both phases in this system, benzoic acid and poly(vinyl stearate), to act as conducting entities therefore resulted in a more complex transport model which takes into account transport contributions from poly(vinyl stearate) as well as isolated and dead end clusters.

The complication produced by the ability of the poly (vinyl stearate) to allow transport of benzoic acid resulted in a nontraditional approach to the determination of the percolation threshold of the system. From ln–ln plots of the experimental bulk diffusivities versus the porosities of all the matrices analyzed, the percolation threshold was taken as the break between two linear regions. From this method, the percolation threshold attributed to the conducting phase of the matrix was determined to be 0.09 ± 0.02, which corresponded to a coordination of 28 ± 7 for the benzoic acid/poly(vinyl stearate) system. The high coordination and low threshold for this system is most likely due to contributions from the complexity of the underlying microstructure as well as the conducting phase associated with the amorphous regions of poly(vinyl stearate).

The mechanisms associated with the observed transport were a combination of percolative transport, or transport along the porous sample-spanning cluster, and cluster diffusion, or transport from cluster to cluster though poly(vinyl stearate) amorphous regions. The cluster diffusion is described in terms of isolated and dead end morphological parameters not normally attributed to transport. Above the percolation threshold, within the concentration range evaluated, the model collapses to the classical percolative transport scheme except for a slight deviation in the direction of higher transport. This slight deviation is assumed real and is hypothesized to be due to enhanced transport caused by jumping from one section of the sample-spanning cluster to another indicative of transport through the polymer.

Although the model developed and analyzed in this paper is simplistic and fits the transport results, the intriguing contributions of finite size scaling combined with free diffusion through amorphous regions of polymers is a topic for future research in this area of drug delivery.

NOMENCLATURE

List of Abbreviations and Variables

Percolation Parameters

$\emptyset$	Porosity
$\emptyset^A$	Volume fraction accessible
$\emptyset^E$	Volume fraction effective or effective diffusivity
$\emptyset_c$	Critical percolation threshold for conducting phase
$\emptyset^I$	Isolated volume fraction
$\emptyset^D$	Dead end cluster volume fraction
$\emptyset^B$	Backbone volume fraction
c	Pre-exponential factor for effective diffusivity scaling relationship
μ	Effective diffusivity scaling relationship exponent
a	Constant for isolated cluster diffusion below percolation threshold
b	Pre-exponential factor for backbone scaling relationship
γ_b	Backbone scaling relationship exponent
z	Number of nearest neighbors or coordination number

Transport and Drug Release Parameters

FBA 4-Fluorobenzoic acid, used as internal reference standard
BA Benzoic acid
D_B Bulk diffusion coefficient (cm^2/s)
D_{aq} Aqueous diffusion coefficient (cm^2/s)
Q Amount of drug released per unit surface area of exposed tablet surface area (mg or g/cm^2)
A Concentration of drug in tablet (g/cm^3)
t Time (s or h)
C_s Solubility of drug in dissolution media (g/ml)
τ Tortuosity
ε Inherent porosity of tablet matrix
ρ Density (g/cm^3)
$\emptyset_d^A$ Drug load or volume fraction accessible due to drug load

Transport Parameters

D Diffusion coefficient through the membrane (cm^2/s)
Q_t Total amount of drug passing through a membrane at time t (mg/cm^2)
l Membrane thickness (cm)
L_t Lag time (days)
C_1 Concentration of drug in the donor compartment

Molecular Weight Determination Parameters

η Intrinsic viscosity (dl/g)
$\overline{M}_v$ Viscosity average molecular weight (Da)

Thermal Analysis Parameters

T_m Melting point (°C)
ΔH_{fus} Enthalpy of fusion (cal/g)

ACKNOWLEDGMENTS

This research was funded in part by the American Chemical Society Chapter of the Petroleum Research Foundation, Glaxo Inc., and the Burroughs Wellcome Fund. The authors would like to thank the constructive feedback provided by the reviewers of this paper. We would also like to express our gratitude to Professor George Zografi for his constant encouragement, support, and outstanding contributions to our scientific field. J.E.H. wishes to dedicate this work to her father, Harold, and husband, Jamshed.

REFERENCES

1. J. E. Hastedt and J. L. Wright. Diffusion in porous materials above the percolation threshold. *Pharm. Res.* **7**(9):893–901 (1990).
2. H. Leuenberger, B. D. Rohera, and Ch. Haas. Percolation theory—a novel approach to solid dosage form design. *Int. J. Pharm.* **38**:109–115 (1987).
3. C. Mallard, J. Coudane, I. Rault, and M. Vert. The use of additives to modulate the release of a sparingly water soluble drug entrapped in PLA50 microparticles. *J. Microencapsul.* **17**(1):81–93 (2000).
4. F. Zhang and J. W. McGinity. Properties of hot-melt extruded theophylline tablets containing poly(vinyl acetate). *Drug Dev. Ind. Pharm.* **26**(9):931–942 (2000).
5. T. Ehtezazi and C. Washington. Controlled release of macromolecules from PLA microspheres: using porous structure topology. *J. Control. Release* **68**:361–372 (2000).
6. I. Caraballo, M. Millán, A. Fini, L. Rodriguez, and C. Cavallari. Percolation thresholds in ultrasound compacted tablets. *J. Control. Release* **69**:345–355 (2000).
7. M. C. Soriano, I. Caraballo, M. Millan, R. T. Pinero, L. M. Melgoza, and A. M. Rabasco. Influence of two different types of excipient on drug percolation threshold. *Int. J. Pharm.* **174**:63–69 (1998).
8. L. M. Melgoza, I. Caraballo, J. Alvarez-Fuentes, M. Millán, and A. M. Rabasco. *Int. J. Pharm.* **170**:169–177 (1998).
9. L. M. Melgoza, A. M. Rabasco, J. Sandoval, and I. Caraballo. Estimation of the percolation thresholds in dextromethorphan hydrobromide matrices. *Eur. J. Pharm. Sci.* **12**:453–459 (2001).
10. J. D. Bonny and H. Leuenberger. Matrix type controlled release systems. I. Effect of percolation on drug dissolution kinetics. *Pharm. Acta Helv.* **66**:160–164 (1991).
11. J. D. Bonny and H. Leuenberger. Matrix type controlled release systems. II. Percolation effects in non-swellable matrices. *Pharm. Acta Helv.* **68**:25–33 (1993).
12. I. Caraballo, M. Fernández-Arévalo, M. A. Holgado, and A. M. Rabasco. Percolation theory: application to the study of the release behaviour from inert matrix systems. *Int. J. Pharm.* **96**:175–181 (1993).
13. I. Caraballo, J. Alvarez-Fuentes, L. M. Melgoza, M. Millán, M. A. Holgado, A. M. Rabasco, and M. Fernandez-Arevalo. Validation study of the conductometrical analysis. Application to the drug release studies from controlled release systems. *J. Pharm. Biomed. Anal.* **18**:281–285 (1998).
14. I. Caraballo, L. M. Melgoza, J. Alvarez-Fuentes, M. C. Soriano, and A. M. Rabasco. Design of controlled release inert matrices of naltrexone hydrochloride based on percolation concepts. *Int. J. Pharm.* **181**:23–30 (1999).
15. H. Leuenberger. New trends in the production of pharmaceutical granules: the classical batch concept and the problem of scale-up. *Eur. J. Pharm. Biopharm.* **52**:279–288 (2001).
16. H. Leuenberger and L. Ineichen. Percolation theory and physics of compression. *Eur. J. Pharm. Biopharm.* **44**:269–272 (1997).
17. T. Kuny and H. Leuenberger. Compression behaviour of the enzyme β-galactosidase and its mixture with microcrystalline cellulose. *Int. J. Pharm.* **260**:137–147 (2003).
18. C. Imbert, P. Tchoreloff, B. Leclerc, and G. Couarraze. Indices of tableting performance and application of percolation theory to powder compaction. *Eur. J. Pharm. Biopharm.* **44**:273–282 (1997).
19. A. F. Rime, D. Massuelle, F. Kubel, H. R. Hagemann, and E. Doelker. Compressibility and compactibility of powdered polymers: poly(vinyl chloride) powders. *Eur. J. Pharm. Bipharm.* **44**:315–322 (1997).
20. T. Zhou, H. Lewis, R. E. Foster, and S. P. Schwendeman. Development of a multiple-drug delivery implant for intraocular management of proliferative vitreoretinopathy. *J. Control. Release* **55**:281–295 (1998).
21. M. Mestiri, J. P. Benoit, P. Hernigou, J. P. Devissaguet, and F. Puisieux. Cisplatin-loaded poly(methyl methacrylate) implants: a sustained drug delivery system. *J. Control. Release* **33**:107–113 (1995).
22. S. R. Ellis. Porous Alumina Ceramics in Drug Delivery: Processing Concerns and Percolation Models. Ph.D. Thesis, School of Pharmacy. University of Wisconsin-Madison, WI (1990).
23. C. D. Mitescu, M. Allain, E. Guyon, and J. P. Clerc. Electrical conductivity of finite-size percolation networks. *J. Phys. A: Math. Gen.* **15**:2523–2531 (1982).
24. G. G. Jerauld, L. E. Scriven, and H. T. Davis. Percolation and conduction on the 3D Voronoi and regular networks: a second case study in topological disorder. *J. Phys. C: Solid State Phys.* **17**:3429–3439 (1984).
25. D. Stauffer. *Introduction to Percolation Theory*, Taylor & Francis, Philadelphia, 1985.
26. A. L. Efros. *Physics and Geometry of Disorder, Percolation Theory*, Mir Publishers, Moscow, 1986.
27. A. Margolina, Z. V. Djordjevic, D. Stauffer, and H. E. Stanley. Corrections to scaling for branched polymers and gels. *Phys. Rev. B.* **28**:1652–1654 (1983).

28. J. E. Hastedt. Diffusional release from a porous polymeric matrix - a model based on percolation theory. M.S. Thesis, School of Pharmacy. University of Wisconsin-Madison, WI (1987).
29. J. E. Hastedt. Percolative transport and cluster diffusion near and below the percolation threshold of a porous polymeric system. Ph.D. Thesis, School of Pharmacy. University of Wisconsin-Madison, WI (1990).
30. KODAK Technical Pan Film 2415/6415 Information. KODAK Publication No. P-255, M6A068 Minor Rev. 2-86-BX, Eastman KODAK Co., Rochester, New York (1985).
31. J. Crank. *The Mathematics of Diffusion*, 2nd ed. Oxford University Press, New York, 1975.
32. W. J. Burlant and A. Adicoff. Polymerization of vinyl stearate by high energy electrons. *J. Polym. Sci.* **27**:269–274 (1958).
33. T. Higuchi. Rate of release of medicaments from ointment bases containing drugs in suspension. *J. Pharm. Sci.* **50**(10):874–875 (1961).
34. T. Higuchi. Mechanism of sustained-action medication. *J. Pharm. Sci.* **52**(12):1145–1149 (1963).
35. R. A. Siegel. Modeling of drug release from porous polymers. In M. Rosoff (ed.), *Controlled Release of Drug: Polymers and Aggregate Systems*, VCH Publishers, New York, 1989, pp. 1–51.
36. G. Grimmett. *Percolation*, Springer, Berlin Heidelberg New York, 1989.
37. S. Kirkpatrick. Percolation and conduction. *Rev. Mod. Phys.* **45**:574–588 (1973).
38. S. Reyes and K. F. Jensen. Percolation concepts in modelling of gas-solid reactions. I. Application to char gasification in the kinetic regime. *Chem. Eng. Sci.* **41**:333–343 (1986).
39. J. Adler, A. Aharony, and D. Stauffer. First exit time of termites and random super-normal conductor networks. *J. Phys. A: Math. Gen.* **18**:L129–L136 (1985).
40. A. Bunde, A. Coniglio, D. C. Hong, and H. E. Stanley. Transport in a two-component randomly composite material: scaling theory and computer simulations of termite diffusion near the superconducting limit. *J. Phys. A: Math. Gen.* **18**:L137–L144 (1985).
41. S. Kirkpartick. In J. C. Garland and D. B. Tanner (eds) AIP Conference Proceedings, No. 40, American Institute of Physics, New York, 1978.
42. C. Domb and N. W. Dalton. Crystal statistics with long-range forces I. The equivalent neighbor model. *Proc. Phys. Soc.* **89**:859–871 (1966).
43. P. Dean and N. F. Bird. *Monte Carlo Studies of the Percolation Properties of Two- and Three-Dimensional Lattices*, National Physics Lab. Math Div. Ma61, Teddington, Middlesex, England, 1966.
44. H. Winterfeld. Percolation and conduction phenomena in disordered composite media. Ph.D. Thesis, University of Minnesota, Ann Arbor, MN, 1981.
45. M. Bohdanecký and M. Netopilík. The Mark-Houwink-Kuhn-Sakurada exponent of polymers with long side groups: is $a_0 = 1/2$ a reliable criterion of the theta state? *Polymer* **36**:3377–3384 (1995).
46. W. S. Port, J. E. Hansen, E. F. Jordan Jr., T. J. Dietz, and D. Swern. Polymerizable derivatives of long-chain fatty acids. IV. Vinyl esters. *J. Polym. Sci.* **VII**:207–220 (1946).
47. F. M. Aliev, K. S. Pojivilko, and V. N. Zgonnik. SAXS and DSC: studies of surface and size effects for poly(vinyl stearate). *Eur. Polym. J.* **26**:101–104 (1990).
48. D. A. Lutz and L. P. Witnauer. Crystallinity of poly(vinyl stearate). *J. Polym. Sci., B, Polym. Lett.* **2**:31–33 (1964).
49. C. A. Oksanen and G. Zografi. The relationship between the glass transition temperature and water vapor absorption by poly(vinylpyrrolidone). *Pharm. Res.* **7**:654–657 (1990).
50. M. Nilsson and M. Strømme. Electrodynamic investigations of conduction processes in humid microcrystalline cellulose tablets. *J. Phys. Chem. B.* **109**:5450–5455 (2005).
51. J. Ricke and G. Reichenauer. Structural investigation of SiO_2—aerogels. *J. Non-Cryst. Solids* **95–96**:1135–1142 (1987).
52. D. Buttner, F. Loffler, R. Caps, and J. Fricke. Investigation of solid thermal conduction in evacuated load-bearing fibrous insulations. *High Temp. High Press.* **18**:537–543 (1986).